Korean J. Chem. Eng., 36(8), 1360-1370 (2019)
DOI: 10.1007/s11814-019-0299-6

pISSN: 0256-1115
eISSN: 1975-7220

Sonocatalytic and photocatalytic efficiency of transition metal-doped ZnO nanoparticles in the removal of organic dyes from aquatic environments

Khosro Hossienzadeh*, Afshin Maleki,†, Hiua Daraei**, Mahdi Safari**, Radheshyam Pawar***, and Seung Mok Lee***,†**

*Student Research Committee, Kurdistan University of Medical Sciences, Sanandaj, Iran
**Environmental Health Research Center, Research Institute for Health Development, Kurdistan University of Medical Sciences, Sanandaj, Iran
***Department of Environmental Engineering, Catholic Kwandong University, Gangneung 25601, Korea
(*Received 5 March 2019 • accepted 15 May 2019*)

Abstract−The present study investigated the efficiency of transition metal-doped ZnO nanoparticles (NPs) in the removal of Direct Blue 71 from aqueous solutions through photocatalytic (UV and visible light) and sonocatalytic processes. The ZnO particles were synthesized and analyzed by the SEM, XRD, FTIR, AFM, DLS, and zeta potential. The reaction conditions were optimized by concerned catalyst (i.e., dopant percentage and catalyst amount), solution pH, catalyst dose and initial dye concentration. The results demonstrated that the Ag-doped ZnO NPs could provide the highest UV light-based photocatalytic efficiency, while the Cu-doped NPs present the greatest sonocatalytic and visible light-based photocatalytic efficiencies. In all processes, the dye removal efficiency was better in acidic pH. Based on the insignificant difference of efficiency over the acidic range of pH, the natural pH of the dye, i.e., 5.6, was considered as the optimal pH value. Also, the increase of dopant percentage enhanced the decolorization efficiency of the catalysts. However, 2.5% dopant amount was selected as the optimal dopant content due to the negligible difference in the decolorization percentages observed using the 2.5 and 5% dopant percentages. Furthermore, the increase of catalyst dose and contact time increased the removal efficiency, while the increase of initial dye concentration resulted in a lower extent of dye decolorization.

Keywords: Photocatalyst, Sonocatalyst, Organic Dye, Transition Metal, ZnO Nanoparticles

INTRODUCTION

Due to the limitation of water resources and development of industrial units, water pollution has turned into one of the most serious environmental concerns [1]. Particularly, the wastewater produced by textile industries contributes significantly to the pollution of water resources [2,3]. Their wastewater discharges contain different dyes and various organic and inorganic compounds [3]. The presence of the dyes is rooted in the fact that around 15% of the total dyes used to dye textiles enter the wastewater [4]. The utilized dyes usually possess one or more benzene rings, which can damage the environment irreversibly due to their toxicity and non-degradability [5]. The issue would get more concerning by knowing that over 700,000 tons of dye materials are produced annually in the world, and about 50% of the produced dyes are azo-dyes. Azo-dyes carry -N=N- moieties in their chemical structures, along with one or several aromatic groups [6,7]. This type of dye is widely applied in the textile, ink, paper, plastic and cosmetics industries [8]. It is while azo-dyes are toxic, carcinogen and mutagen for aquatic species [9].

There are different methods for removal of dyes from wastewaters, including biological treatment [10], coagulation [11], adsorption [12,13], membrane processes [14] and advanced oxidation processes (AOPs) [15,16]. Adsorption and coagulation transfer the contaminants from the aqueous phase to a solid phase; furthermore, they do not decompose the contaminant molecules [17]. On the other hand, photocatalytic and sonocatalytic AOPs, which rely on semiconductor nanoparticles (NPs), have attracted much interest since they are low-cost, non-toxic and chemically stable [18-20]. Among various semiconductor NPs, zinc oxide (ZnO) has gained more attention due to its high optical sensitivity, non-toxicity, high stability, wide bandgap energy and great efficiency in electron generation [15]. The mechanism of photocatalytic decomposition of ZnO is based on the absorption of light (with energy equal to or exceeding the band gap energy (Eg) of ZnO) by photocatalyst and its excitation. Consequently, it causes the formation of a positive hole (p^+) in the valence band and an electron (e^-) in the conduction band. The positive hole is a potent oxidizing agent that can directly oxidize contaminants or, through the decomposition of water molecules and the production of strong hydroxyl radicals, it extends the process of degradation of almost all organic pollutants with no selectivity [21,22].

However, the use of pure ZnO nanoparticles for the photocatalytic process has two major disadvantages. The first is the high recombination rate of the photogenerated electron-hole pairs, and the second is related to its photostability in an aqueous medium. These

†To whom correspondence should be addressed.
E-mail: maleki43@yahoo.com, leesm@cku.ac.kr

problems significantly reduce the photocatalytic activity of pure ZnO and limit the application of this semiconductor in photocatalytic processes. The addition of transition metals to pure ZnO is a promising method to enhance photocatalytic response to the visible light and decrease electron-hole recombination [23].

Although ZnO has many advantages, its properties and applicability can be further improved by doping [24]. Doping of ZnO with an appropriate dopant can change its bandgap energy and prevent recombination of charge carriers (electron-hole pairs), which promotes its efficiency in photocatalytic and sonocatalytic degradation of organic and toxic pollutants [25,26]. Since the state and reduction energy level of many transition metals lies within the bandgap energy of ZnO, doping a transition metal ion into ZnO structures generates new electronic levels from the conduction band (CB) to the valence band (VB) of ZnO. The generation of such levels enables absorption of visible light and charge transition from the d orbital of the dopant to the CB or VB of ZnO [27]. Concerning the advantages of doping ZnO, Ruh et al. [28] doped ZnO with Mn and investigated visible-light induced degradation of dyes. Their results showed that Mn-dopant could increase the photocatalytic activity of ZnO.

Direct Blue 71 (DB71) is a water-soluble organic compound that is classified as an Azo dye, and is used as a common dye in the textile, paper, leather, polyester, cotton, and silk industries and therefore easily release to the environment through different effluents and leads to various environmental problems [29,30]. Also, potential toxicity and carcinogenicity of azo dyes have also been reported, and therefore their presence in the water resources is a concern and a health threat [30]. For this reason, their treatment and removal before the entering into the environment has always been considered, and so far different methods have been used for this purpose. For example, Saien and Soleymani used UV/TiO_2 process to decompose DB71, and yielded 97% removal efficiency [29]. Ertugay and Acar studied the sonophotocatalytic degradation of DB71 in the presence of ZnO and observed that the combination of UV and ZnO was an effective process for the destruction of DB71, and the color removal yield was 100% [31]. In another study, removal of DB71 by electrocoagulation sludge recycling in photo-Fenton process was done and its results showed that in optimum conditions of photo-Fenton process 96.27% decolorization was achieved [1]. Therefore, due to the importance of the subject, the purpose of this study was to synthesize transition metal-doped ZnO nanoparticles and determine their sonocatalytic and photocatalytic efficiency in DB71 removal from aquatic environments.

METHODS AND MATERIALS

1. Chemicals

The organic dye with the commercial name of Direct Blue 71 (DB 71) was purchased from Alvan Sabet Company (Iran). $Zn(NO_3)_2 \cdot 6H_2O$, $Ce(SO_4)_2 \cdot 4H_2O$, $(CH_3COO)_3 \cdot Mn \cdot 2H_2O$, $(CH_3COO)_2 \cdot Cu \cdot H_2O$ and $Ag(NO_3)$ were purchased from Merck (Germany). The pH of the solutions was adjusted by adding NaOH and H_2SO_4 (Merck). All chemicals were of analytical grade.

2. Reactor

The present lab-scale experiments were performed using a closed system and a glassy reactor with 250 mL capacity. The photocatalytic experiments in the UV region were carried out using two 15-W UV lamps (Philips, Netherlands) by fixing them at the top of the reactor. For the visible region experiments natural sunlight was used as the light source. The sonocatalytic process was carried out using an Elema ultrasonic device (Germany) at 37 kHz frequency and 100% power.

3. Photocatalyst Synthesis

To synthesize the un- and Ag-, Cu-, Mg- and Ce-doped ZnO nanocatalysts, a solvothermal method was used [32]. To prepare the un-doped ZnO product, first, 119 g/*l* (0.4 M) hexahydrate zinc nitrate and 54.18 g/*l* (0.6 M) oxalic acid were dissolved separately in 100 mL deionized water and heated to the boiling point of the solutions. Then, the oxalic acid solution was added gradually to the zinc nitrate solution. The mixture was placed on a shaker and stirred for one h, at (±5) 65 °C, then, cooled to room temperature. The obtained fine homogeneous ZnO particles were then washed several times with distilled water, exposed to air for 24 h and dried for five h in an oven at 100 °C. In the next step, the Ag-doped ZnO particles were prepared using the described procedure. The only difference was that 5 mL of silver nitrate solution of 0.15 M concentration was added gradually to the zinc nitrate solution before the addition of the oxalic acid solution. To synthesize the Ce-, Cu-, Mn-, CuMn-, CuCe-, CeMn-, CuAg-, MnAg- and CeAg-doped ZnO (with dopant concentration of 2.5%), first the zinc nitrate solution was prepared with the mixing of 0.15 M silver nitrate, including 0.3 M $Mn(CH_3COO)_2 \cdot 4H_2O$, 0.25 M $Cu(CH_3COO)_2$ and 0.115 M $Ce(SO_4)_2 \cdot 4H_2O$ were mixed. After that, the oxalic acid solution was introduced to the above-prepared solution. The other synthesis steps of un-doped ZnO followed [33]. For the synthesis of other percentages of dopant, including 0.25, 0.5, 1 and 5% for each of the metals, molar amounts of 0.015, 0.03, 0.06 and 0.3 for Ag, 0.0115, 0.023, 0.046 and 0.23 for Ce, 0.03, 0.06, 0.12 and 0.6 for Mn, and 0.025, 0.05, 0.1 and 0.5 were used with the above method, respectively. To synthesize co-doped ZnO nanocatalyst, all of the above values were used as described above.

4. Efficiency Assessment of the Samples

The photocatalytic performance of the as-synthesized particles was tested by observing the degradation performance of Direct Blue 71 dye. A stock solution of DB 71 (1,000 mg/*l*) was made by dissolving DB 71 in distilled water and stored in a refrigerator at 4 °C. The maximum absorbance wavelength (λ_{max}) of DB 71 was determined as 585 nm and used to quantify the amount of the dye before and after each treatment and calculate removal efficiency through Eq. (1). In Eq. (1), C_{in} and C_{out} are the initial and final concentrations of DB 71, respectively [34,35].

$$R = \left(1 - \frac{C_{out}}{C_{in}}\right) \times 100 \quad (1)$$

The effect of the photocatalytic process on decolorization of DB 71 was deteremined in the presence of UV two 30-W UV lamps. The process was optimized by considering the operational parameters of catalyst type, dopant concentration (0.1, 0.5, 1.0, 2.0 and 5.0 g/*l*), initial dye concentration (20, 100, 200 and 300 mg/*l*) and contact time (30, 60, 90, 120 and 180 min). The visible light-based process was performed in the peak hours of sunshine by exposing the sam-

ple solutions to visible light under optimized operational parameter of UV light.

Similarly, to evaluate the effect of ultrasound waves on decolorization of DB 71, an ultrasonic path with 37 kHz frequency and 100% power was employed. The process was optimized by concerning catalyst type, dopant percentage (0.25, 0.5, 1.0, 1.5 and 5.0%), solution pH (3, 5, 7, 9 and 11), catalyst dose (0.1, 0.5, 1.0, 2.0 and 5.0 g/*l*), initial dye concentration (20, 100, 200 and 300 mg/*l*) and contact time (30, 60, 90, 120 and 180 min).

5. Particle Characterization

A MIRA3 Tuscan (Czech) scanning electron microscope (SEM) was used to discover the particle shape and size of the ZnO samples. X-ray diffraction (XRD) spectroscopy by an EQUINOX 3000 Intel device (France) was employed to study the crystalline structure and order of the samples. Total organic carbon (TOC) of the samples were determined using a TOC analyzer, Formacs^{HT} (Skalar Analytical, The Netherlands). The surface structure and properties of the NPs were determined using an atomic force microscopy (AFM) instrument (model: Advance, Ara Pazhoohesh Co., Iran). Zeta potential of the samples was measured by a Nanobrook device (Brookhaven, USA) to determine their surface charge and colloidal properties.

RESULTS AND DISCUSSION

1. Characterization

The SEM images of the 2.5% Cu- and Ag-doped ZnO nanoparticles are shown in Fig. 1. The Digimizer software was utilized to measure the particle size of the nanoparticles. Based on the obtained SEM images, ZnO NPs are composed of hexagonal morphology [36]. Also, while the Cu-doped ZnO NPs are non-aggregated (Fig. 1(a)), the Ag-doped ZnO NPs are agglomerated (Fig.

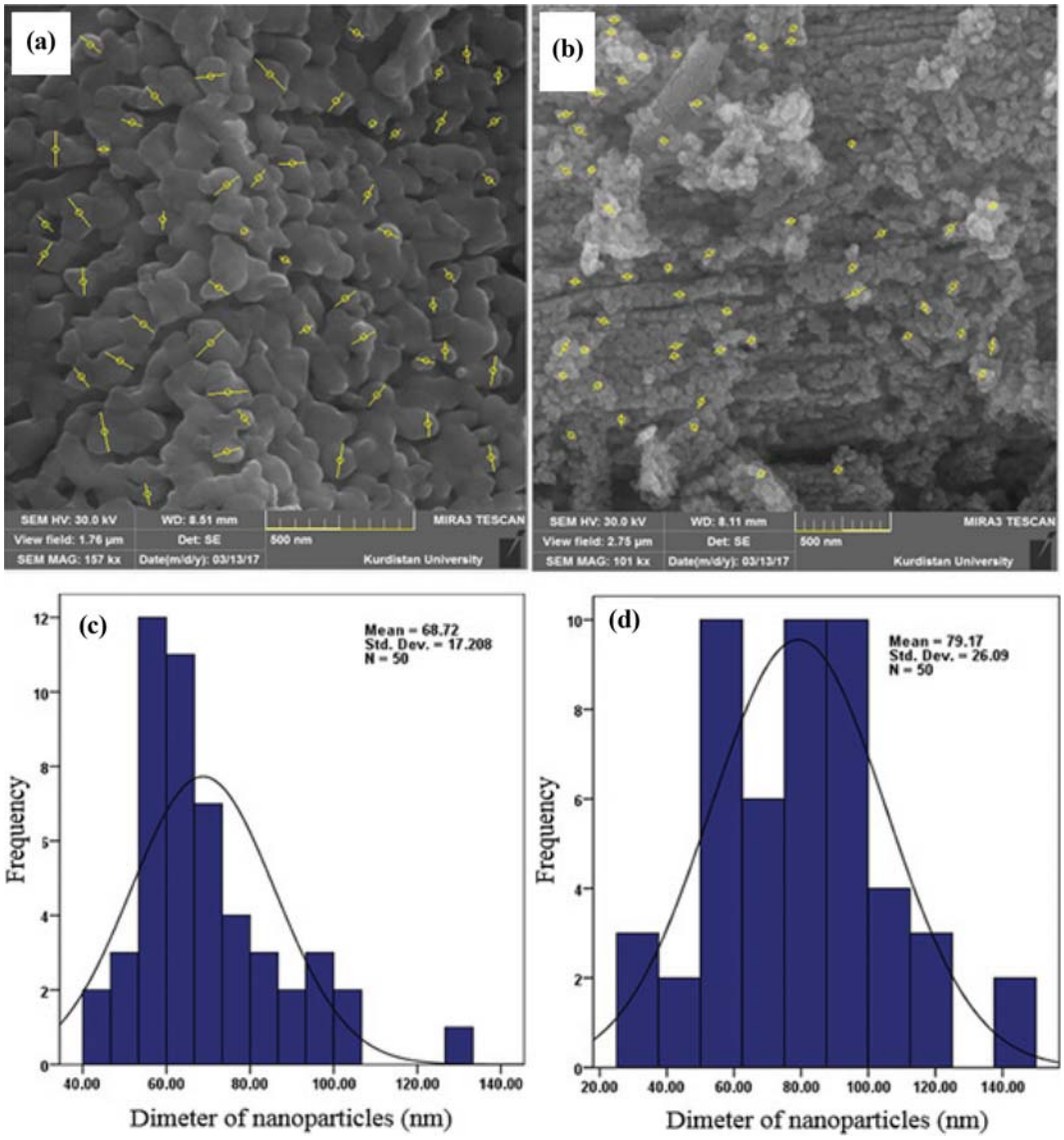

Fig. 1. SEM images of the Cu-doped (a) and Ag-doped (b) ZnO particles, Size distribution of the Cu-doped (c) and Ag-doped (d) ZnO particles (with 2.5% dopant percentage).

1(b)). Fig. 1(c), (d) also shows the average size and standard deviation associated with the two ZnO samples. According to this figure, the Cu-doped particles are 68.72±17.208 nm in size, while the size of the Ag-doped ZnO particles is 91.19±26.09 nm.

The XRD spectra of the samples were recorded to obtain some information about their crystalline structure and phases. The XRD patterns of the un- and Ag-, Ce-, Cu-, MnZn-, CuMn-, CuCe-, CeMn-, CuAg- and MnAg-doped ZnO samples are exhibited in Fig. 2.

As can be seen, all XRD patterns contain three main peaks related to the (100), (002) and (101) crystal planes. These peaks are consistent with that of pure ZnO particles (JCPDS stand card No. 800075) [37] and represent hexagonal crystal lattice. Besides, the patterns outline no impurity phase corresponding to the dopant metals, such as Ag, Cu, AgO, Ce, Mn, CuO, ZnOAgO and ZnO-CuO. However, the presence of the dopants has resulted in a shift of the XRD peaks due to the substitution of the Zn^{2+} ions by metal ions with greater effective ionic radii and expansion of the lattice network.

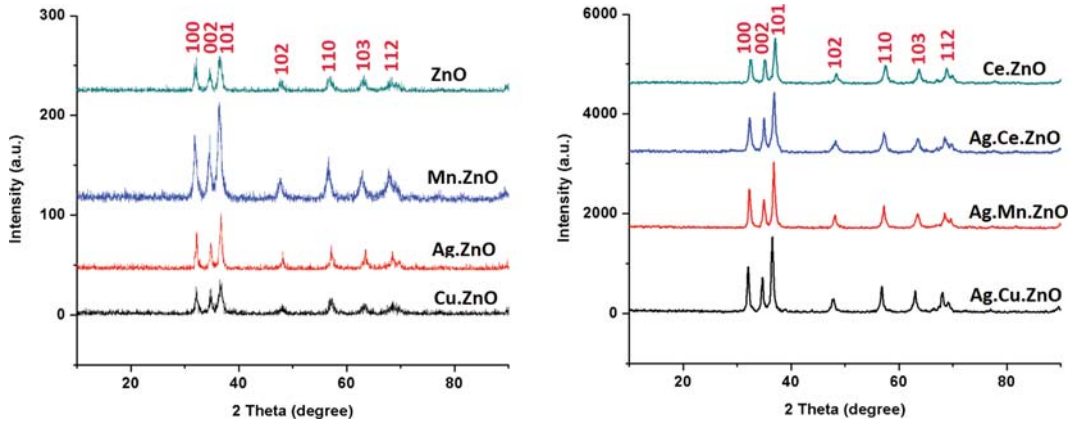

Fig. 2. XRD patterns of the synthesized particles (with 2.5% dopant percentage).

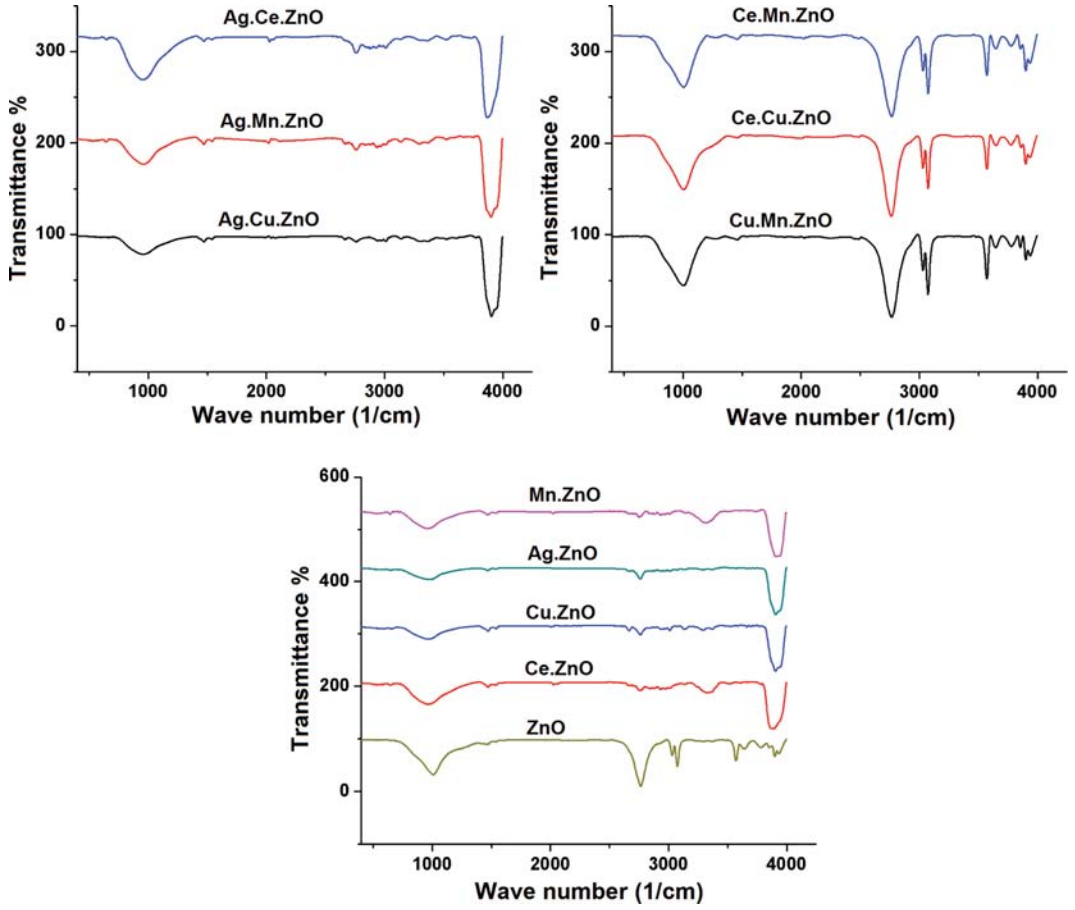

Fig. 3. FTIR spectra of the synthesized particles.

The most intense peaks are observed around 36.045° and refer to the (101) plane [37].

The functional groups of the undoped ZnO NPs and Ag-, Ce-, Cu-, MnZn-, CuMn-, CuCe-, CeMn-, CuAg- and MnAg-doped ZnO NPs were confirmed through FTIR spectroscopy. The resultant FT-IR spectra are demostrated in Fig. 3. According to the spectra, all samples have given rise to a strong vibrational band at 469 cm^{-1} that corresponds to Zn-O stretching [38]. At 1,730 cm^{-1}, the stretching vibration of C=O confirms the presence of organic materials. Also, C-H and N-H stretching vibrations of the amine groups appear at 3,000 and 3,448 cm^{-1}. Similar vibrational bands referring to Zn-O and N-H stretching have also been reported in other works about doped ZnO particles, e.g. [33], over the 600 to 400 cm^{-1} and 3,600 to 3,400 cm^{-1} frequency ranges, respectively.

The AFM images of the Cu- and Ag-doped NPs are shown in Fig. 4. These topographical images declare the presence of NPs on the surface of the two samples and suggest that the dx parameter, which indicates particle size, equals to 78 and 46 nm for the Ag- and Cu-doped ZnO particles, respectively. Also, they estimate the relative roughness of the Ag- and Cu-doped samples (Rq) as 1.0623 and 1.1696 nm.

UV-Vis spectrometry is the most reported technique for evaluating the optical properties and examining the doping effects on the host metal oxide matrix [39]. For this reason, the optical properties of the pure and metal-doped ZnO were evaluated with UV-vis spectrometry and results shown in Fig. 5. It is clear that the absorption edge of metal-doped samples shifts toward the visible light region in comparison to pure ZnO. So, clearly it turns out that the metal dopants successfully entered into the ZnO nanoparticle crystal network and effectively extended absorption of ZnO into the visible light range.

Zeta potential can be used to study the distribution of potential

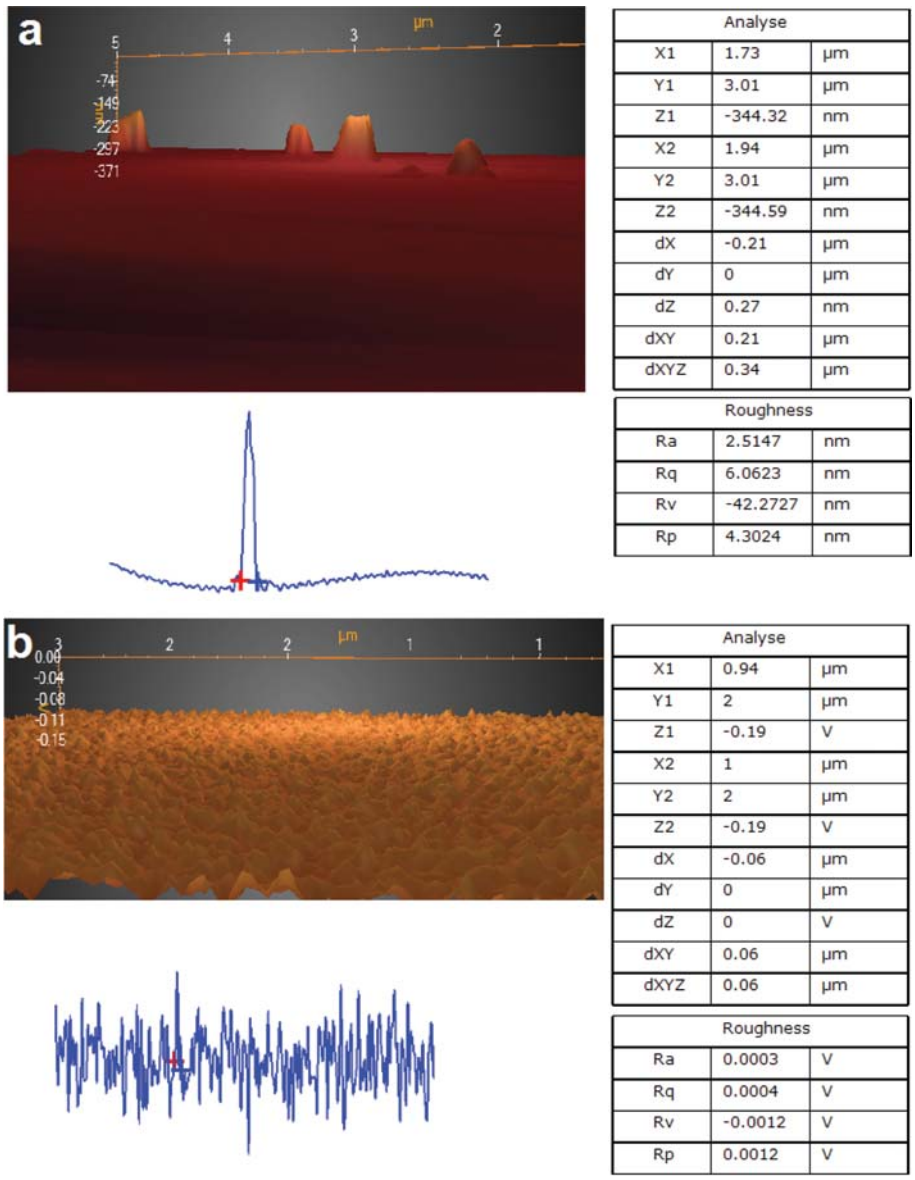

Analyse		
X1	1.73	µm
Y1	3.01	µm
Z1	-344.32	nm
X2	1.94	µm
Y2	3.01	µm
Z2	-344.59	nm
dX	-0.21	µm
dY	0	µm
dZ	0.27	nm
dXY	0.21	µm
dXYZ	0.34	µm

Roughness		
Ra	2.5147	nm
Rq	6.0623	nm
Rv	-42.2727	nm
Rp	4.3024	nm

Analyse		
X1	0.94	µm
Y1	2	µm
Z1	-0.19	V
X2	1	µm
Y2	2	µm
Z2	-0.19	V
dX	-0.06	µm
dY	0	µm
dZ	0	V
dXY	0.06	µm
dXYZ	0.06	µm

Roughness		
Ra	0.0003	V
Rq	0.0004	V
Rv	-0.0012	V
Rp	0.0012	V

Fig. 4. The AFM image of the Ag-doped (a) and Cu -doped (b) ZnO NPs (with 2.5% dopant percentage).

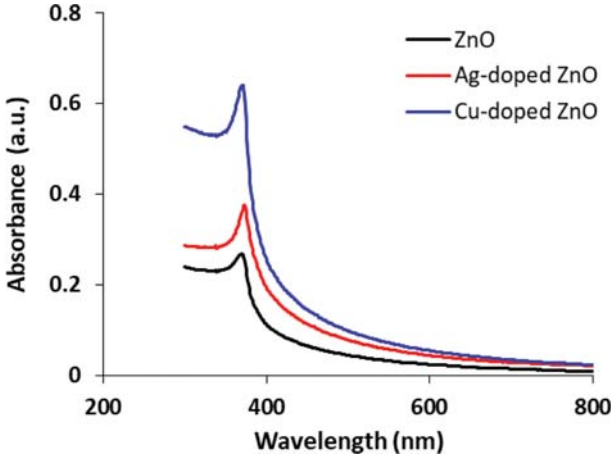

Fig. 5. UV-Vis absorption spectra of the pure ZnO, Ag-doped ZnO and Cu-doped ZnO nanoparticles.

at the interface of colloids. Also, it can help to determine the tendency of particles towards aggregation in solutions. These parameters were calculated in the presence of simple ions and complicated systems, such as surface-active materials, multivalent ions, polymers, and proteins. For this reason, the electrostatic zeta potential of dendrimer was measured using principles of phase analysis light scattering (PALS) and electrophoretic light scattering (ELS), and its result in Table 1 and Fig. 6. Table 1 presents the electric potential of the synthesized NPs. According to the values reported in Table 1, doping ZnO increases its zeta potential and mobility. So that, the zeta potential of Ag-, Cu-, Ce-, Mn- and un-doped ZnO is −8.69, −9.71, −11.75, −12.40 and −10.66 mV, respectively. The highest increase of surface charge refers to the Mn.Ce-doped ZnO NPs with −17.21 mV zeta potential.

Dynamic light scattering (DLS) is a physical, fast and non-destructive technique that can be employed to determine the distribution of particles in solutions and suspensions. This method is adopted for particle sizes ranging from several nanometers to several microns. Based on the DLS results (Fig. 6), the Ag- and Cu-doped NPs are smaller and distributed more homogeneously, relative to the un-doped ZnO NPs.

Table 1. Zeta potential (PALS method) details of bare and doped ZnO NPs using the Smoluchowski model

Sample	Zeta potential (mV)	Mobility (μ/s)/(V/cm)
ZnO	−10.66	−0.83
Ce.ZnO	−11.75	−0.92
Cu.ZnO	−9.71	−0.76
Ag.ZnO	−8.69	−0.68
Mn.ZnO	−12.4	−0.97
Cu.Mn.ZnO	−9.25	−0.72
Cu.Ce.ZnO	−10.67	−0.83
Ce.Mn.ZnO	−17.21	−1.34
Cu.Ag.ZnO	−6.81	−0.53
Mn.Ag.ZnO	−3.33	−0.26
Ce.Ag.ZnO	−10.42	−0.81

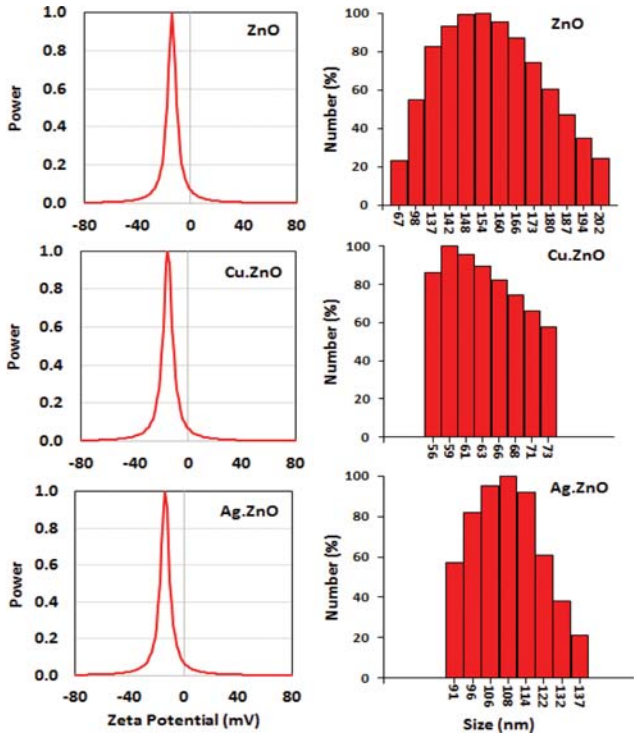

Fig. 6. Zeta potential (ELS method) and DLS results of ZnO NPs (with 2.5% dopant percentage).

2. The Catalytic Efficiency of the ZnO Samples in Dye Decolorization Under UV, Visible and Ultrasound Irradiation

To investigate the decolorization efficiency of the synthesized NPs under UV light, visible light and ultrasound irradiations and choose the best catalyst type, several sample solutions containing 100 mg/*l* DB 71 dye and 2 g/*l* ZnO NPs with 2.5% dopant percentage were exposed to UV light, visible light and ultrasound waves at pH 7.0. The obtained results are presented in Fig. 7. The highest UV and visible light-based photocatalytic activity corresponds to the Ag- and Cu-doped ZnO NPs and equals to 73.5 and 55.5%, respectively. Also, the greatest sonocatalytic decolorization, i.e., 73%, is observed for the Cu-doped sample. These samples were chosen as the optimal catalyst in further experiments. The noticeable performance of these two samples was attributed to their specific functional groups and high roughness (see Fig. 4), which enhance the distribution and adsorption of the DB 71 molecules onto their surface [40]. Inconsistency with these results, Özlem et al. [41] reported that doping ZnO NPs with Ag improves their photocatalytic efficiency.

3. Effect of Dopant Concentration on Decolorization Efficiency

After selection of the Ag- and Cu-doped NPs as the most efficient ZnO samples, the optimal molar percentages of the Ag and Cu dopants were determined. In this respect, the 0.25, 0.5, 1.0, 2.5 and 5.0 molar percentages were evaluated. As Fig. 8 demonstrates, increasing the concentration of the dopants improves the decolorization efficiency of all examined processes. So that, applying 2.5 and 5% of the dopant mentioned above gives the decolorization efficiencies of 79.3 and 81.1%, 85.53 and 87.7%, and 75.89 and 81.02% under irradiation of UV light, visible light and ultrasound

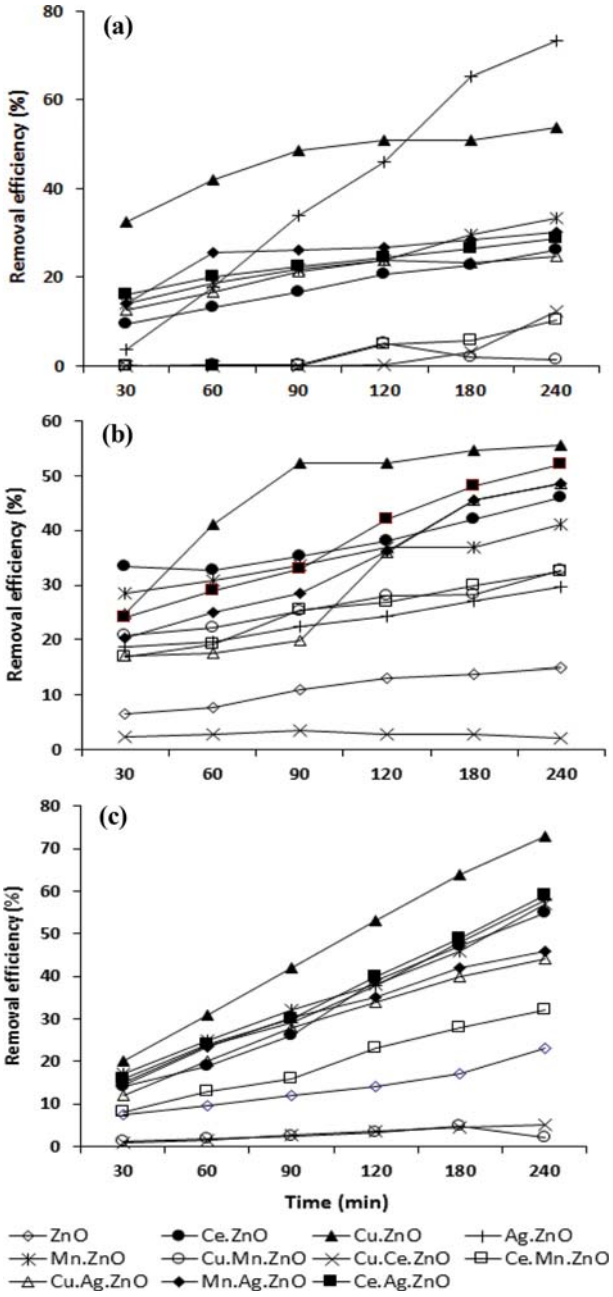

Fig. 7. Decolorization efficiency of the ZnO NPs under UV light (a), visible light (b) and ultrasound (c) irradiation (30 W UV light, 100 mg/*l* dye concentration, 2 g/*l* catalyst dose, pH 7.0 and 2.5% dopant percentage).

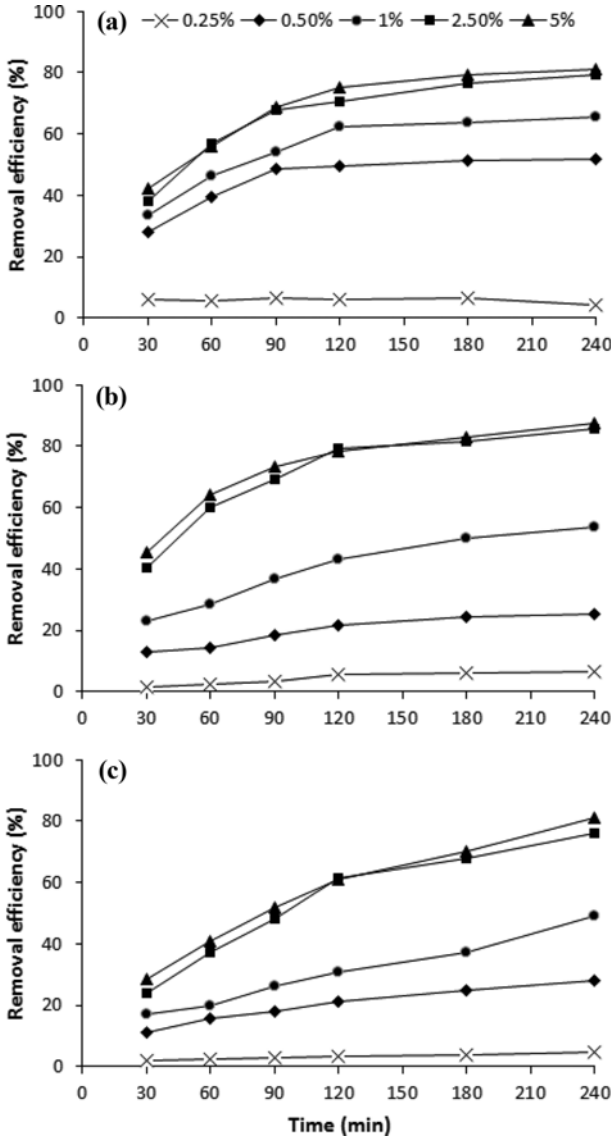

Fig. 8. Effect of dopant percentage on decolorization efficiency of the UV light irradiated (30 W) Ag-doped ZnO NPs (a), visible light irradiated Cu-doped ZnO NPs (b) and ultrasonicated Cu-doped ZnO NPs (c) using 100 mg/*l* dye concentration, 2 g/*l* catalyst dose and pH 7.0.

waves, respectively. These values suggest that increasing the dopant concentration from 2.5 to 5.0% does not lead to any significant improvement in the catalytic activity of the three processes. This statement is also evident from Fig. 8, in which increasing the dopant content of the NPs can considerably promote the DB 71 decolorization percentage just up to the dopant percentage of 2.5%. Therefore, 2.5% of dopant was considered as the optimal dopant concentration.

Other researchers have reported similar types of findings of dopant concentration. For instance, Djaja et al. [42] stated that increasing the concentration of the Ce dopant in the synthesized ZnO NPs up to a particular level increases the photocatalytic efficiency and decreases it by utilizing higher Ce contents. The reason for the decolorization enhancement observed by using higher dopant percentages is that doping decreases the bandgap energy of the NPs and increases their photocatalytic activity in response to light.

4. Effect of pH

The influence of solution pH for the three catalytic procesas ses wevaluated in the several ranges of pH such as pH 3, 5, 7, 9 and 11. According to the results presented in Fig. 9, at pH 3, 5, 7, 9 and 11, the decolorization percentages related to UV-based photocatalysis are 76.8, 80.6, 69.9, 64.0 and 59.0%, the results associated with visible light-based photocatalysis are 86, 82.5, 66, 53.9 and 30, and the efficiencies of the sonocatalytic process are 77, 70, 56, 44 and

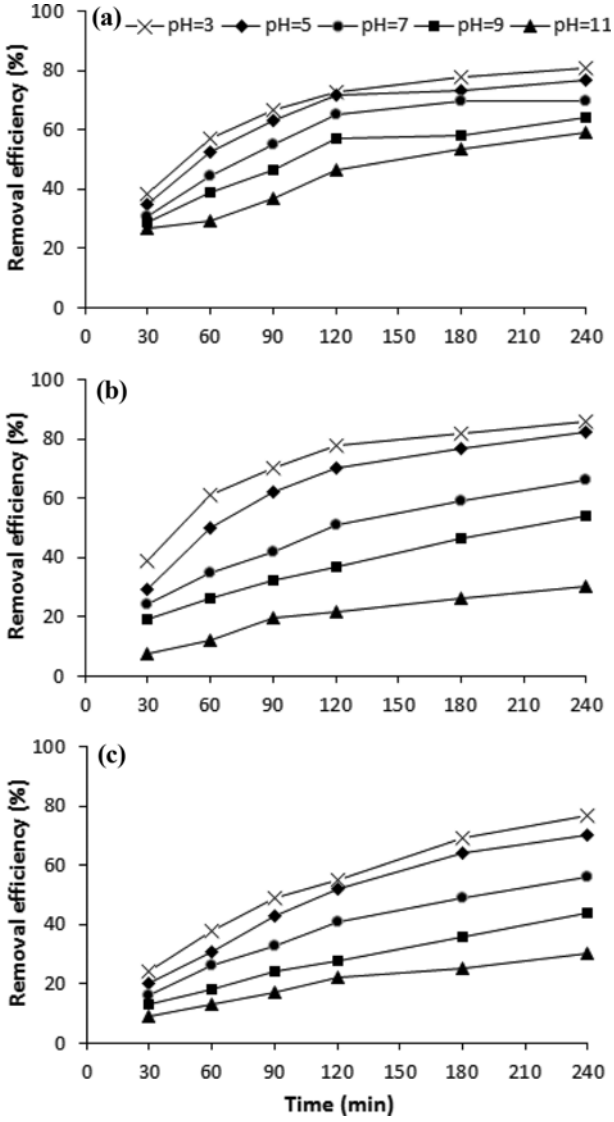

Fig. 9. Effect of pH on decolorization efficiency of the UV light irradiated (30 W) Ag-doped ZnO NPs (a), visible light irradiated Cu-doped ZnO NPs (b) and ultrasonicated Cu-doped ZnO NPs (c) using 100 mg/*l* dye concentration, 2 g/*l* catalyst dose and 2.5% dopant percentage.

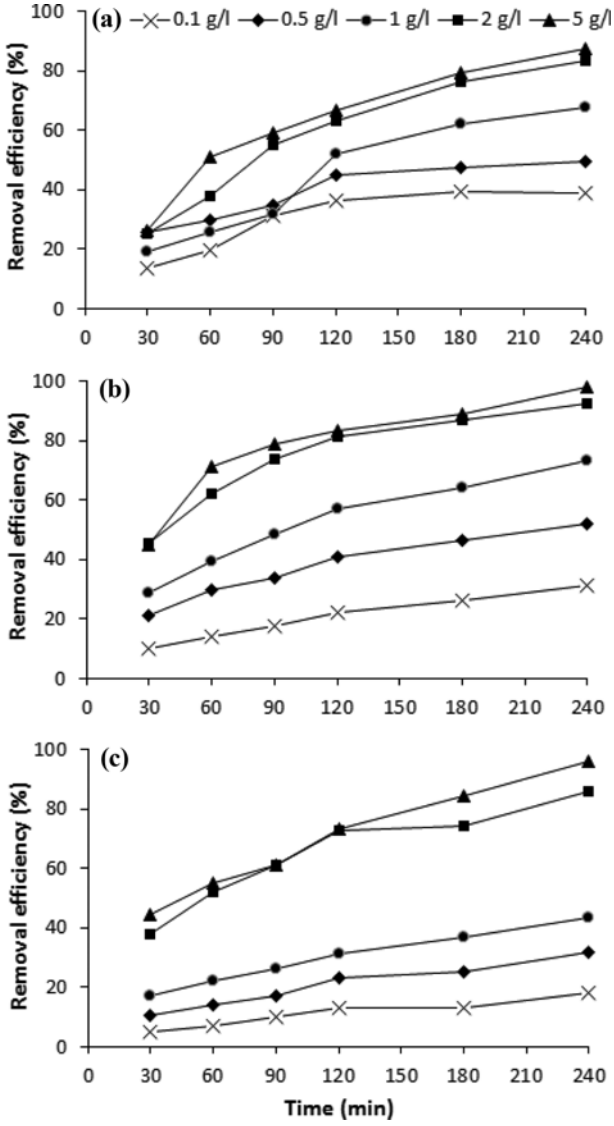

Fig. 10. Effect of catalyst dose on decolorization efficiency of the UV light irradiated (30 W) Ag-doped ZnO NPs (a), visible light irradiated Cu-doped ZnO NPs (b) and ultrasonicated Cu-doped ZnO NPs (c) using 100 mg/*l* dye concentration, pH 5.6 and 2.5% dopant percentage.

30%, respectively. Consequently, the activity of the processes is relatively similar at the 3 and 5 pH levels. So that, the efficiencies observed at pH 3 and 5 using UV light, visible light and ultrasound are, respectively, 76.8 and 80.6%, 86.0 and 82.5%, and 77 and 70%. Therefore, the closer to neutral pH such solution pH (5.6) of DB 71 dye solution was chosen as the optimal pH. The increase of efficiency at acidic conditions is due to the dominant electrical charges on the surface of ZnO NPs at such conditions [43]. The other reason is facilitated production of OH radicals via the interaction of the H^+ ions with superoxide radical. On the other hand, at basic conditions, the efficiency decreases due to the fast decomposition of OH radicals [31]. A similar impact of pH on photocatalytic and sonocatalytic removal of organic dyes was reported by Maleki et al. [44], who worked on decolorization of Reactive Black 5 and Distress Orange 25 and concluded that acidic pH enhances degradation of the two dyes.

5. Effect of Catalyst Dose

The influence of optimized catalyst dose amount on decolorization of DB 71 dye was evaluated by varying the catalyst amount in the range of 0.1-55 g/*l*. The observed results are displayed in Fig. 10, which shows that increasing the catalyst dose improves decolorization of DB 71 by the three processes. The increase of catalyst dose is so effective that the decolorization percentages observed after 240 min contact time using 0.1, 2 and 5 g/*l* of the ZnO NPs are, respectively, 39.02, 83.1 and 87.14% for the UV light-based process, 31.14, 92.4 and 97.8% in the presence of visible light, and 18.0, 85.67 and 95.8% under ultrasound irradiation. As these values, the efficiency of DB 71 removal promotes sharply with the increase of

catalyst dose from 0.1 to 2.0 g/*l* due to the provision of a higher number of active catalytic sites and, consequently, increased generation of OH and other oxidative radical [45].

On the other hand, increasing the dose from 2 to 5 g/*l* improves the decolorization efficiency negligibly. Therefore, the catalyst concentration of 2 g/*l* was selected as the optimal catalyst dose. Inconsistent with these results, former studies have shown that increasing the amount of catalyst increases removal efficiency up to a definite limit and, after that, the additional NPs might diffract the irradiated light rays and decrease decolorization efficiency [31]. Note that high catalyst doses are not examined since they would cause solution turbidity, light scattering, and prevention of light penetration, which would decrease photodegradation [46]. Also, in the sonocatalytic process that utilizes ultrasound waves as the energy source for NP activation, the NPs have a great tendency towards aggregation due to their high surface area and surface energy. However, the ultrasound waves diffuse the particles to prevent their aggregation. It is while the effectiveness of the ultrasonication process decreases when the concentration of the NPs is very high [31].

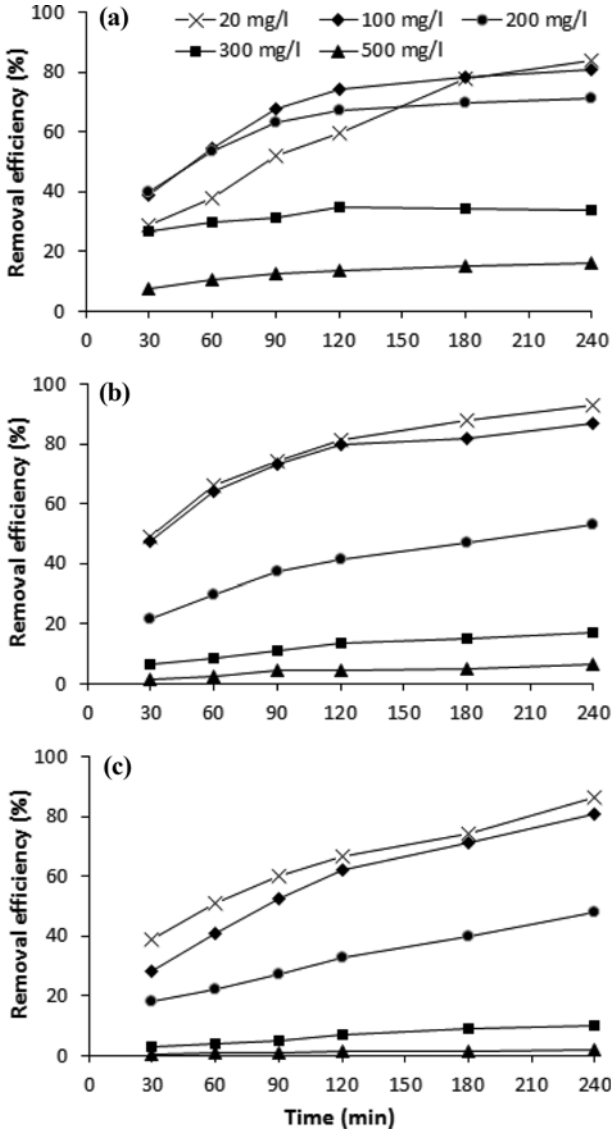

Fig. 11. Effect of initial dye concentration on decolorization efficiency of the UV light irradiated (30 W) Ag-doped ZnO NPs (a), visible light irradiated Cu-doped ZnO NPs (b) and ultrasonicated Cu-doped ZnO NPs (c) using 2 g/*l* catalyst dose, pH 5.6 and 2.5% dopant percentage.

6. Effect of Initial Dye Concentration

To investigate the impact of initial dye concentration on decolorization efficiency was demonstrated by varying the DB 71 solution concentrations in the range of 20-500 mg/*l* and the obtained results are exhibited in Fig. 11.

Concerning this figure, the increase of DB 71 concentrations decreases the decolorization efficiency of all examined processes. To be more specific, adopting the dye concentrations of 20, 200 and 500 mg/*l* within 240 min provides the removal percentages of 84, 71.1 and 16.2% in UV light-based catalysis, 93, 53 and 6.5% in the visible light-based photocatalytic process, and 86.16, 48 and 1.93% in the sonocatalytic system, respectively. The reason is that increasing the number of pollutant molecules results in the occupation of a greater number of active catalyst sites, decreased generation of oxidant radicals and reduced rate of decolorization [15]. Moreover, according to the Beer-Lambert law, light transmission through solutions decreases with the increase of dye concentration and the light rays get absorbed and trapped by the dye molecules instead of the catalyst particles. As an outcome, OH generation by the catalyst and degradation of the DB 71 molecules is reduced.

The decrease of photocatalytic degradation efficiency with the increase of pollutant concentration has been reported by many ZnO-based wastewater treatment studies, e.g. [47,48]. Also, the catalytic degradation of pollutants has been explained based on the generation of active OH radicals [49]. Barakat declared that increasing dye concentration in wastewater decreases removal efficiency since it causes solution turbidity and decreases active surface area as the dye molecules adsorbed on the catalyst particles [50].

7. Effect of Contact Time

The effect of contact time (30, 60, 120, 180 and 240 min) on decolorization efficiency of the photocatalytic and sonocatalytic processes was investigated at all levels of pH, catalyst dose and dye concentration. It was revealed that prolonging contact time improves the efficiency of DB 71 decolorization in all studied processes. So that, at 30, 60, 90, 120, 180 and 240 min, the UV light-based treatment results in 25, 38, 54.8, 63.3, 76.19 and 83.1% removal percentage, the visible light-based process gives 20.4, 39.5, 48.4, 64 and 73.1% efficiency, and sonocatalysis presents 25.2, 35, 52, 61, 72.69 and 75.35% decolorization, respectively. The reason is that the impact of light rays on the surface of the catalyst particles leads to the release of electron pairs. Therefore, increasing the contact time would produce more electrons and OH radicals, and the OH radicals would have sufficient time to degrade the dye molecules.

Consequently, longer contact times can enhance removal efficiency. In agreement with this finding, Khorram Abadi et al. observed increased photocatalytic decolorization of methylene blue by ZnO NPs with the increase of contact time [51]. They reported that decolorization efficiency and COD removal increases from 6 and 1.8% to 100 and 82% by increasing the contact time from 5 to 130 min, respectively. They attributed the reason to the provision of adequate time for generation of OH radicals, attack of the gen-

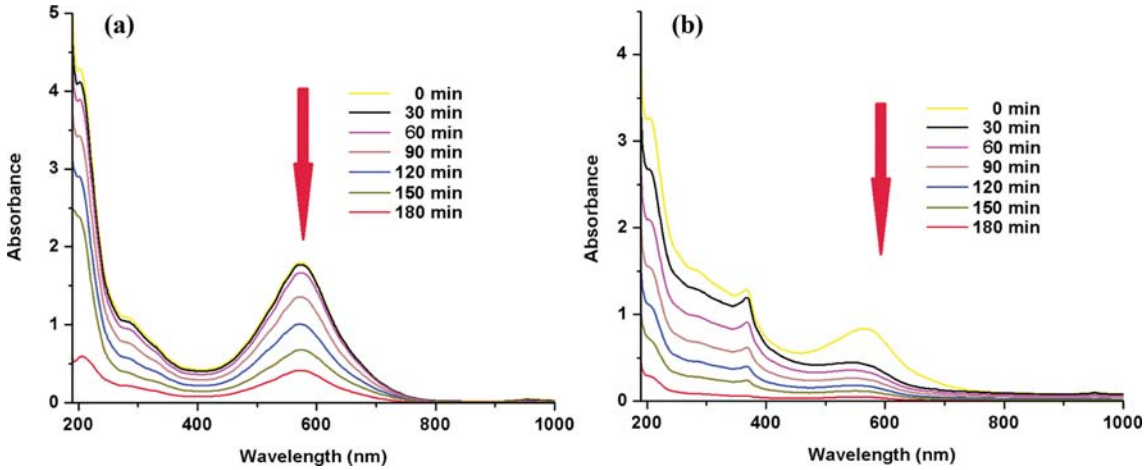

Fig. 12. UV-vis absorbance spectra of Direct Blue 71 dye after different time intervals at (a) photocatalytic process with Ag-doped ZnO NPs and (b) sonocatalytic process with Cu-doped ZnO NPs using 2 g/*l* catalyst dose, pH 5.6, and 2.5% dopant percentage.

erated radicals to the dye molecules and progress of the reaction.

Direct Blue 71 dye absorption in the photocatalytic process with Ag-doped ZnO NPs and sonocatalytic process with Cu-doped ZnO NPs at different time intervals was analyzed using a UV-Vis spectrophotometer at a wavelength of 190-1,100 nm, and the results are shown in Fig. 12. These results show the maximum absorption of Direct Blue 71 dye is in the visible region at a 585 nm wavelength. As the irradiation time continued, the intensity of Direct Blue 71 absorption peak started decreasing for both processes, but the downward trend for the sonocatalytic process was much more severe and completely disappeared after 180 minutes. The disappearance of the absorption peak in the visible region suggests that decolorization occurred through the destruction of the main chromophores of the dye and as a result the solution became colorless. In assessing the sonocatalytic process, samples showed a high percentage decolorization of 100% in 180 min and completely got decolorized. However, as shown in Fig. 11, catalytic activity increased with increasing reaction time, and more than 80% efficiency was observed in dye decolorization. But that does not mean that the destruction of dye had happened. On the other hand, the amount of mineralization during the process is another important point which should be considered. For this reason, the amount of total organic carbon (TOC) in the processes examined at different time intervals was determined and their results are presented in Fig. 13. According to these results, it is clear that in the sonocatalytic process, about 55% of mineralization had taken place. So, although a complete decolorization has happened, there are still intermediate compounds derived from dye degradation in the aquatic environment and therefore require a special sensitivity to discharge into the environment.

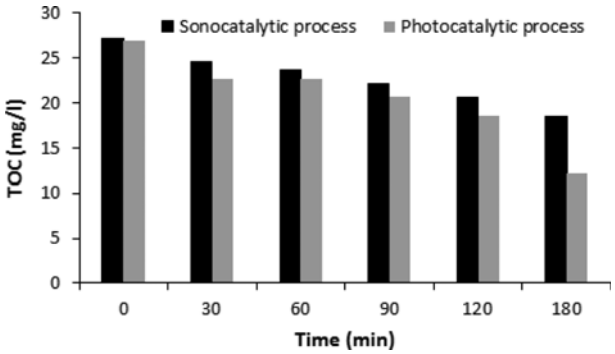

Fig. 13. Total organic carbon of Direct Blue 71 dye after different time intervals at (a) photocatalytic process with Ag-doped ZnO NPs and (b) sonocatalytic process with Cu-doped ZnO NPs using 2 g/*l* catalyst dose, pH 5.6 and 2.5% dopant percentage.

CONCLUSION

The results indicate the effects of doping the zinc oxide nanoparticles lattice with diverse transition metals on its characteristics, e.g., size, shape, surface, lattice, FTIR spectra, zeta potential, and especially photo/sono catalytical activities in decolorization of Direct Blue 71. The study mostly shows enhancing influence on the photo/sono activity of zinc oxide while a number of them cause to quenching effect. The result is in agreement with previously reported theoretical and practical studies and confirms the capability of doping process to control the characteristics and efficiency of zinc oxide as an environmentally friendly catalyst mainly for its application for water and wastewater treatment. The enhanced photo/sono catalytical activity of modified zinc oxide is promising as a greener solution for organic pollution degradation using renewable energy of solar irradiation and without need to adjust the pH for the process.

ACKNOWLEDGEMENT

This study was extracted from a Master's dissertation which was supported by Kurdistan University of Medical Sciences (IR.MUK.REC.1395/41) and approved by the Environmental Health Research Center. Hereby, we extend our gratitude to the sponsors of this study.

REFERENCES

1. M. Moradi, A. Eslami and F. Ghanbari, *Desalination Water Treat.*, **57**(10), 4659 (2016).
2. N. Daneshvar, S. Aber, V. Vatanpour and M. H. Rasoulifard, *J. Electroanal. Chem.*, **615**(2), 165 (2008).
3. A. Al-Kdasi, A. Idris, K. Saed and C. T. Guan, *Global Nest: the Int. J.*, **6**(3), 222 (2004).
4. G. Moussavi and M. Mahmoudi, *J. Hazard. Mater.*, **168**(2), 806 (2009).
5. R. Jiraratananon, A. Sungpet and P. Luangsowan, *Desalination*, **130**(2), 177 (2000).
6. E. M. Saggioro, A. S. Oliveira, T. Pavesi, C. G. Maia, L. F. V. Ferreira and J. C. Moreira, *Molecules*, **16**(12), 10370 (2011).
7. L. Rizzo, *Water Res.*, **45**(15), 4311 (2011).
8. M. Dutta, P. Ghosh and J. K. Basu, *J. Taiwan Inst. Chem. Engineers*, **43**(6), 879 (2012).
9. R. L. Singh, P. K. Singh and R. P. Singh, *Int. Biodeterior. Biodegrad.*, **104**, 21 (2015).
10. S. M. d. A. G. Ulson, K. A. S. Bonilla and A. A. U. de Souza, *J. Hazard. Mater.*, **179**(1-3), 35 (2010).
11. B. Shi, G. Li, D. Wang, C. Feng and H. Tang, *J. Hazard. Mater.*, **143**(1-2), 567 (2007).
12. G. Crini and P.-M. Badot, *Prog. Polym. Sci.*, **33**(4), 399 (2008).
13. S. Yavari, N. M. Mahmodi, P. Teymouri, B. Shahmoradi and A. Maleki, *J. Taiwan Inst. Chem. Engineers*, **59**, 320 (2016).
14. J.-S. Wu, C.-H. Liu, K. H. Chu and S.-Y. Suen, *J. Membr. Sci.*, **309**(1-2), 239 (2008).
15. A. Jonidi Jafari, R. Rezae Kalantari, M. Gholami and A. Esrafili, *Iranian J. Health Environ.*, **5**(2), 167 (2012).
16. A. H. Mahvi and A. Maleki, *Desalination Water Treat.*, **20**(1-3), 197 (2010).
17. S. Alijani, M. Vaez and A. Zaringhalam Moghadam, *Iranian J. Health Environ.*, **6**(2), 243 (2013).
18. M. A. Zazouli, M. Ahanjan, Y. Kor, M. Eslamifar, M. Hosseini and M. Yousefi, *J. Mazandaran Univ. Med. Sci.*, **25**(122), 227 (2015).
19. S. Abo-Farha, *J. Am. Sci.*, **6**(10), 128 (2010).
20. B. Shahmoradi, M. Negahdary and A. Maleki, *Environ. Eng. Sci.*, **29**(11), 1032 (2012).
21. Y. Wang, Q. Wang, X. Zhan, F. Wang, M. Safdar and J. He, *Nanoscale*, **5**(18), 8326 (2013).
22. A. Gutierrez-Mata, S. Velazquez-Martínez, A. Álvarez-Gallegos, M. Ahmadi, J. A. Hernández-Pérez, F. Ghanbari and S. Silva-Martínez, *Int. J. Photoenergy*, **2017** (2017).
23. R. D. C. Soltani, G. Shams Khoramabadi, H. Godini and Z. Noorimotlagh, *Desalination Water Treat.*, **56**(9), 2551 (2015).
24. K. M. Joshi, B. N. Patil, D. S. Shirsath and V. S. Shrivastava, *Adv. Appl. Sci. Res.*, **2**(3), 445 (2011).
25. O. Mekasuwandumrong, P. Pawinrat, P. Praserthdam and J. Panpranot, *Chem. Eng. J.*, **164**(1), 77 (2010).
26. A. Maleki and B. Shahmoradi, W*ater Sci. Technol.*, **65**(11), 1923 (2012).
27. L. Palmisano, V. Augugliaro, A. Sclafani and M. Schiavello, *J. Phys. Chem.*, **92**(23), 6710 (1988).
28. R. Ullah and J. Dutta, *J. Hazard. Mater.*, **156**(1-3), 194 (2008).
29. J. Saien and A. Soleymani, *J. Hazard. Mater.*, **144**(1-2), 506 (2007).
30. N. Mirzaei, A. H. Mahvi and H. Hossini, *Adsorpt. Sci. Technol.*, **36**(1-2), 80 (2018).
31. N. Ertugay and F. N. Acar, *Appl. Surf. Sci.*, **318**, 121 (2014).
32. M. Samarghandi, M. Siboni, A. Maleki, S. J. Jafari and F. Nazemi, *J. Mazandaran Univ. Med. Sci.*, **21**(81), 44 (2011).
33. B. Subash, B. Krishnakumar, R. Velmurugan, M. Swaminathan and M. Shanthi, *Catal. Sci. Technol.*, **2**(11), 2319 (2012).
34. J. Müslehiddinoğlu, Y. Uludağ, H. Ö. Özbelge and L. Yilmaz, *J. Membr. Sci.*, **140**(2), 251 (1998).
35. J. Yoon, G. Amy, J. Chung, J. Sohn and Y. Yoon, *Chemosphere*, **77**(2), 228 (2009).
36. H. Xu, H. Wang, Y. Zhang, W. He, M. Zhu, B. Wang and H. Yan, *Ceram. Int.*, **30**(1), 93 (2004).
37. H. Sowa and H. Ahsbahs, *J. Appl. Crystallogr.*, **39**(2), 169 (2006).
38. C. L. Bahena, S. S. Martínez, D. M. Guzmán and M. d. R. T. Hernández, *Chemosphere*, **71**(5), 982 (2008).
39. W. Guo, Y. Shen, G. Boschloo, A. Hagfeldt and T. Ma, *Electrochim. Acta*, **56**(12), 4611 (2011).
40. G. A. Al-Dahash, Q. M. Salman and M. F. Haddawi, *J. Kerbala Univ.*, **15**(2), 87 (2017).
41. Ö. A. Yıldırım, H. E. Unalan and C. Durucan, *J. Am. Ceram. Soc.*, **96**(3), 766 (2013).
42. N. F. Djaja and R. Saleh, *Mater. Sci. Applications*, **4**(02), 145 (2013).
43. C.-H. Wu, *Dyes Pigm.*, **77**(1), 31 (2008).
44. A. Maleki, A. H. Mahvi, R. Ebrahimi and Y. Zandsalimi, *Korean J. Chem. Eng.*, **27**(6), 1805 (2010).
45. I. K. Konstantinou and T. A. Albanis, A*ppl. Catal. B: Environ.*, **49**(1), 1 (2004).
46. M. Behnajady, N. Modirshahla and R. Hamzavi, *J. Hazard. Mater.*, **133**(1), 226 (2006).
47. S. Pardeshi and A. Patil, *J. Mol. Catal. A: Chem.*, **308**(1), 32 (2009).
48. M. Qamar and M. Muneer, *Desalination*, **249**(2), 535 (2009).
49. D. F. Ollis, E. Pelizzetti and N. Serpone, *Environ. Sci. Technol. (United States)*, **25**(9), 1522 (1991).
50. M. Barakat, *J. Hydro-environment Res.*, **5**(2), 137 (2011).
51. Z. Noorimotlagh, G. Shams, H. Godini and R. Darvishi, *Yafteh*, **14**(5), 51 (2013).